Applied Physics Letters

Formation of controllable 1D and 2D periodic surface structures on cobalt by femtosecond double pulse laser irradiation

Cite as: Appl. Phys. Lett. **115**, 031601 (2019); https://doi.org/10.1063/1.5103216
Submitted: 25 April 2019 . Accepted: 26 June 2019 . Published Online: 16 July 2019

Sohail A. Jalil, Jianjun Yang, Mohamed ElKabbash, Cong Cong, and Chunlei Guo

Applied Physics Letters ARTICLE scitation.org/journal/apl

Formation of controllable 1D and 2D periodic surface structures on cobalt by femtosecond double pulse laser irradiation

Cite as: Appl. Phys. Lett. **115**, 031601 (2019); doi: 10.1063/1.5103216
Submitted: 25 April 2019 · Accepted: 26 June 2019 ·
Published Online: 16 July 2019

Sohail A. Jalil,[1,2] Jianjun Yang,[1,a)] Mohamed ElKabbash,[3] Cong Cong,[3] and Chunlei Guo[1,3,a)]

AFFILIATIONS

[1]State Key Laboratory of Applied Optics, Changchun Institute of Optics, Fine Mechanics and Physics, Chinese Academy of Sciences, Changchun 130033, China
[2]University of Chinese Academy of Sciences, Beijing 100049, China
[3]The Institute of Optics, University of Rochester, Rochester, New York 14627, USA

[a)]**Authors to whom correspondence should be addressed:** jjyang@ciomp.ac.cn and guo@optics.rochester.edu

ABSTRACT

Controlling the surface morphology at the subwavelength scale is one of the cornerstones of modern nanophotonics. Femtosecond laser-induced surface structuring is a viable technique for the large-scale formation of nano- and microscale structures. A typical example is the formation of one-dimensional laser-induced periodic surface structures (LIPSSs), which can lead to strong modifications of optical and wetting properties of the material surface. Creating two-dimensional (2D) patterned structures, however, is a more challenging and rewarding task. Here, we demonstrate a single step method for fabricating various subwavelength structures on the cobalt (Co) surface using different laser fluences (0.12–0.24 J/cm^2) and time delay (0–30 ps) between double pulses. More importantly, we can control the geometry and organization of the formed structures demonstrating spherical, triangular, rhombic, and high spatial frequency LIPSSs using two temporally delayed orthogonally polarized femtosecond laser beams. We show that the laser fluence and delay time between the two beams are the controlling parameters for realizing the different surface morphologies. We provide a numerically supported, phenomenological model to explain the formed 2D structures. Our model employs elements from both the scattered surface-wave interference and the self-organization theories that are commonly used to explain uniform surface structures.

The creation of subwavelength structures is of paramount importance to modern photonics and surface functionalization where surface morphological features can effectively manipulate the optical[1] and mechanical[2] properties of materials with various potential applications including surface wetting properties,[3] magnetic recording media,[4] catalysts for hydrogen energy,[5] sensings,[6] and plasmonics.[7] Traditional nanofabrication tools such as electron beam and focused ion beam lithography suffer from high cost and low throughput.[8–10] On the other hand, ultrafast laser processing has been broadly adopted as an alternative tool for the formation of nano- and microscale structures suitable for a wide range of applications in photonics, plasmonics, and optoelectronics.[3,11–13] Compared to complex lithographic methods, femtosecond laser processing has many advantages as a direct laser writing technique suitable for almost all types of materials. In particular, femtosecond laser processing usually does not require masks, templates, or a specialized clean room environment.[3,11,13–15] Ultrafast laser surface-processing can successfully produce different types of subwavelength structures including nano- and microscale structures, holes and craters, conical, and columnar structures, 1D and 2D microstructures, and femtosecond laser-induced periodic surface structures (fs-LIPSSs).[3,16] Among these structures, fs-LIPSSs were extensively studied as they offer a facile way of achieving well-organized and highly precise patterns.[17–20] Fs-LIPSSs were used to demonstrate a wide range of applications such as structural coloring,[1] perfect light absorption,[21] antireflective surfaces, and improved wetting properties.[3,22,23] The underlying mechanism of fs-LIPSSs is commonly believed to be a result of interference between the incident light and the scattered surface waves, namely, surface plasmons (SPs).[3,15]

To this end, the realization of 1D fs-LIPSS structures is a widely studied area to understand their creation mechanism and, consequently, control the morphology and period of fs-LIPSSs. Under fixed spot irradiation, the dynamics of 1D fs-LIPSSs were studied on

Titanium using single- and two-color double-fs-pulse experiments.[24] On the other hand, in the scanning mode, the formation of 2D fs-LIPSSs was recently demonstrated using circularly polarized light[25,26] and using two temporally delayed fs-laser pulses.[27–31] By adopting these methods, 2D periodic microstructure arrays were formed,[27–29] which provides an effective way of creating subwavelength 2D structures.[3,28,32] However, so far, only one geometry of 2D structures was produced for a given laser processing technique and the origin of such structures remains elusive.

In this study, we demonstrate a single step method for fabricating 1D and 2D subwavelength structures with a wide range of shapes including spherical, triangular, rhombic, and high spatial frequency LIPSS (HSFL) by using only two temporally delayed, orthogonally polarized, femtosecond laser beams on a bulk Co surface. We show that the laser fluence and the time delay between the two pulses provide controls for creating different kinds of structures. Investigating the parameter space for temporally delayed pulses allowed us to provide a framework to understand the emergence of such structures and shows that the dominant mechanism in the structure formation depends on the laser fluence. For each type of surface structure, optimal processing conditions are obtained experimentally as a function of the laser fluence and the time delay between the two laser beams.

A schematic diagram of the experimental setup is shown in Fig. 1, where two temporally delayed pulses are interacting with the Co surface to create a permanent pattern (see supplementary material note 1 and Fig. S1, for more details).

To determine the effect of using a double pulse femtosecond laser in realizing uniform fs-LIPSSs, we first investigate the formation of single pulsed fs-LIPSSs at various laser processing parameters. A well-defined fs-LIPSS structures showed a periodicity of $\Lambda^{\text{Single beam}} \sim (550 \pm 20)$ nm, using $F = 0.17\,\text{J/cm}^2$, V = 0.30 mm/s, and a distance of 300 μm from the focal point (see the supplementary material, Fig. S2, for more details).

In order to fabricate different types of surface microstructures, we carried out two sets of experiments, varying fluence while keeping the delay time constant and varying the time delay while keeping the fluence constant. Within 0 ps $< \Delta t <$ 30 ps, we varied the fluence and obtained various 2D surface structures, where the fluence of an individual laser beam is sufficiently below the uniform 2D structural threshold of the surface. For all double pulse experiments, the linear polarizations of the first and the second laser beams were kept along the vertical and horizontal directions, respectively.

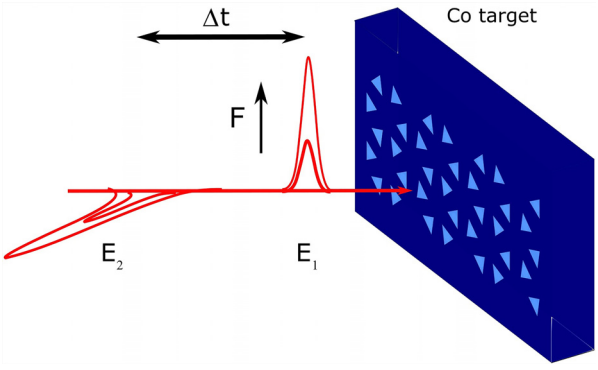

FIG. 1. A schematic diagram for the formation of subwavelength structures on the Co surface, using two temporally delayed femtosecond laser beams with orthogonal linear polarization. Here, Δt represents the time delay of two beams arriving onto the target surface, whereas E_1 and E_2 show the cross-polarization of two laser beams. The vertical arrow shows the increase in the value of laser fluence (F). The pulse duration is 35 fs, the wavelength is 800 nm, the laser repetition rate is 1 kHz, and the focusing distance is 300 μm before the sample.

Figure 2 shows the different geometries obtained by varying these parameters. The damage and uniform fs-LIPSS threshold for Co are experimentally obtained to be 0.09 J/cm^2 and 0.14 J/cm^2, respectively. For $F < 0.14\,\text{J/cm}^2$, we only obtain random nanoroughness as shown in Fig. 2(a) ($F = 0.12\,\text{J/cm}^2$ and $\Delta t = 4$ ps). Similarly, for short delay times, $\Delta t < 4$ ps, we obtain random nanostructures that suffer from over melting, i.e., the induced melting led to the lack of uniformity, as shown in Fig. 2(b) ($F = 0.20\,\text{J/cm}^2$ and $\Delta t = 2$ ps).

Several 2D periodic structures are formed within the delay time window of 4ps $< \Delta t <$ 12ps. The zoom-in view of 2D periodic surface structures is shown in the supplementary material, Fig. S3. Spherical nanostructures organized in a square lattice with 2D periodicity are formed for $0.14\,\text{J/cm}^2 < F < 0.18\,\text{J/cm}^2$. Figure 2(c) shows the formation of submicron spherical structures at $F = 0.14\,\text{J/cm}^2$ and $\Delta t =$ 12 ps. Random nanostructures and HSFL are formed over the spherical structures. The individual sphere diameter is (540 ± 40) nm, and the measured horizontal and the vertical periodicities are (643 ± 30) nm and (670 ± 30) nm, respectively. In addition, vertical periodic lines forming due to E_2 are more pronounced than the horizontal periodic lines due to the dominance of the second pulse in ablating the material surface as was previously demonstrated.[33]

By increasing the net fluence of the two laser beams to $F = 0.20\,\text{J/cm}^2$ and $\Delta t = 12$ ps, triangular structures are formed and are organized in a honeycomb lattice, referred hereinafter as honeycomb packed triangles (HPTs), as shown in Fig. 2(d), where individual structural units are delineated by periodic lines in three distinct directions constituting the submicron triangular structures. The outline of the structural unit presents a triangular shape, with side lengths of approximately (400 ± 20) nm. The vertical, left slanted, and right slanted periodicities are (670 ± 40) nm, (669 ± 40) nm, and (647 ± 30) nm, respectively. Within such surface structures, only vertical periodic ridges and valleys are oriented perpendicular to the polarization direction of the second laser beam, while the other two periodic ridges and valleys, i.e., left slanted and right slanted, are oriented neither parallel nor perpendicular to any of the two laser polarization directions. The triangular particle edges face one another such that each particle is surrounded by three other particles and the triangles' three edges face each other, i.e., there is no vortex facing an edge in any of the formed structures.

By further increasing the net fluence to $F = 0.24\,\text{J/cm}^2$ and Δt = 12 ps, rhombic structures are formed as shown in Fig. 2(e). The rhombic structures are formed with left slanted and right slanted periodicities of (720 ± 40) nm and (740 ± 40) nm, respectively. The rhombic structures are also periodic; however, the formed structures are neither perpendicular nor parallel to both pulses' polarizations.

By increasing the delay time further, we observe the formation of HSFL with deep subwavelength periodicities, ($F > 0.22\,\text{J/cm}^2$ and 14 ps $< \Delta t <$ 26 ps) [Fig. 2(f)]. The complete evolution of HSFL structures with increasing Δt at $F = 0.22\,\text{J/cm}^2$ can be seen in the supplementary material, Fig. S4. HSFL structures were reported before by laser ablation, and the period of HSFL was 4.2–5.1 times smaller than

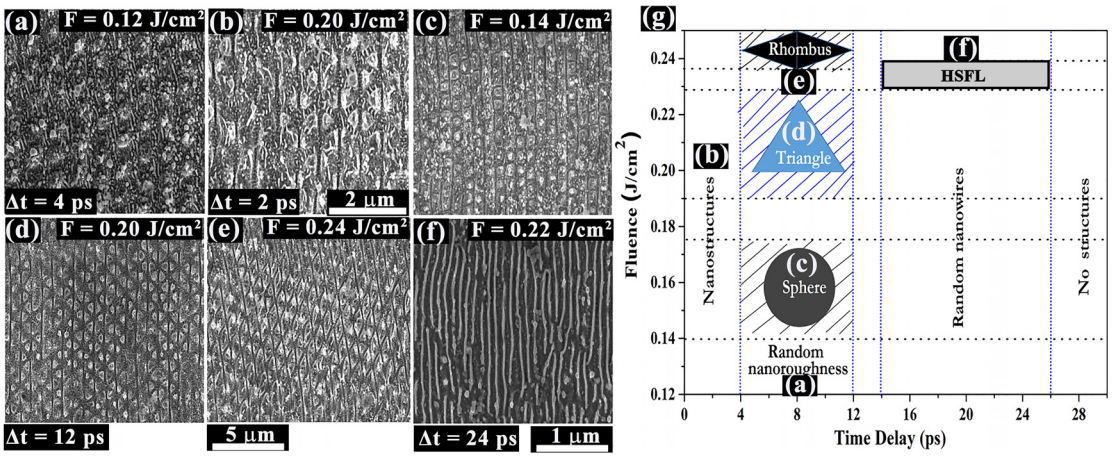

FIG. 2. SEM images of 1D and 2D surface structures with different laser fluences and time delays, under irradiation of two temporally delayed femtosecond laser beams: (a) Random nanoroughness at $F = 0.12$ J/cm^2 and $\Delta t = 4$ ps. (b) Extensive nanostructures at $F = 0.20$ J/cm^2 and $\Delta t = 2$ ps. Evidently, uniform patterning of the surface does not occur for short delay times $\Delta t < 4$ ps and low laser fluence $F < 0.14$ J/cm^2. (c)–(e) SEM images for the evolution of 2D surface structures with different laser fluences, under irradiation of two temporally delayed femtosecond laser beams at a constant time delay of $\Delta t = 12$ ps. Formation of spherical, honeycomb packed triangular, and rhombic structures at (c) $F = 0.14$ J/cm^2, (d) $F = 0.20$ J/cm^2, and (e) $F = 0.24$ J/cm^2, respectively. The scale bar of 5 μm is the same as for (c)–(e). (f) Formation of 1D HSFL on the Co surface at the fluence of $F = 0.22$ J/cm^2 and the time delay of 24 ps between the two laser beams. (g) The parameter space for surface structures formed (a)–(f) due to temporally delayed double pulse laser ablation.

the laser wavelength.[34] However, in our case, the period of HSFL is 8.42 times smaller than the incident wavelength. The produced HSFL can be used as metafilms for high absorption application. Initially, at $\Delta t = 17$ ps, nanodroplets are formed (see the supplementary material, Fig. S5, for zoom-in view). At $\Delta t = 24$ ps, the HSFL length and width are (2500 ± 20) nm and (50 ± 10) nm, respectively, [Fig. 2(f)], i.e., they have an aspect ratio of ~50. The vertical alignment of the HSFL is perpendicular to the polarization direction of the delayed incident laser beam, E_2. The HSFL period is (95 ± 25) nm, indicating that these are type II-HSFL which occurs for materials with strong light absorption, e.g., Ti and Ni. The observed period (95 ± 25) nm of the periodic HSFL is comparable to the previous report on Ti (140 nm).[24] Figure 2(g) summarizes the optimal conditions for the formation of the different 2D periodic surface structures, in terms of the laser fluence and time delay of the two laser beams.

The formation mechanism of the 2D square lattice fs-LIPSSs is fairly similar to the well-established 1D grating fs-LIPSSs. According to the electromagnetic theory of fs-LIPSS formation, interference between the incident light and the surface scattered wave, here surface plasmon polaritons (SPPs), leads to a periodic modulation of the laser intensity on the ablated material surface which creates periodic surface structures with orientation determined by the laser polarization.[35] For two temporally delayed pulses with orthogonal polarizations, the orthogonally polarized pulses create orthogonal interference patterns, thus forming a square lattice.[27,28]

While the microrhombic structures were not reported before using direct fs-laser writing, the HPT structures have been reported by us[29] and others.[25,26] The origin of HPT structures, however, remains elusive as the scattered-surface wave theory of fs-LIPSSs cannot explain the orientation and geometry of the formed structures. It was suggested that they are a result of hexagonal convection flow patterns in the molten material after laser irradiation.[25] While this is an intriguing explanation, it does not explain the origin of the hexagonal flow pattern nor the triangular shape of the individual surface structures. In general, HPT structure formation requires using single circularly polarized light[26] or double cross polarized beams.[29] Accordingly, it is clear that having two temporally delayed, orthogonally polarized fields is a necessary, but not sufficient, condition to fabricate HPT structures. We note here that using circularly polarized light can generate hexagonal-shaped arrangements in specific conditions; however, it cannot form different structures as a function of laser fluence and delay time.[25,26]

Here, we propose a phenomenological model, supported by numerical simulations, which explains the square lattice, HPT, and rhombic structures while taking into account the aforementioned observations summarized in Fig. 2(g). Our experiments show that HPT structures require higher laser fluence than the spherical structures organized in a square lattice. Initially, we obtain structures formed in a transient square lattice as expected from the conventional scattered wave-SPP interference mechanism [Fig. 3(a)]. The particles organized in a square lattice then will turn into HPT structures by self-organization due to Coulomb repulsion between molten surface structures after subsequent irradiation.[36] Note that this Coulomb repulsion is simply due to surface charge acquired following the fs-laser pulse which ionizes the material surface[35] and is not the well-known nonthermal melting Coulomb explosion phenomenon.[37,38] This repulsive force pushes the particles to form in a hexagonal lattice [Fig. 3(b)]. This further explains why the structures are edge-facing triangles; the repulsion between the molten structures will flatten the edges; since each structure, in a simple hexagon, has three nearest neighbors, they form triangular particles. By considering the viscosity force of the molten surface and the Coulomb repulsive forces, we can simulate the distribution of a number of particles with an identical mass and charge having a square lattice as an initial condition and study the system evolution using the second order Euler method, given as follows:[39]

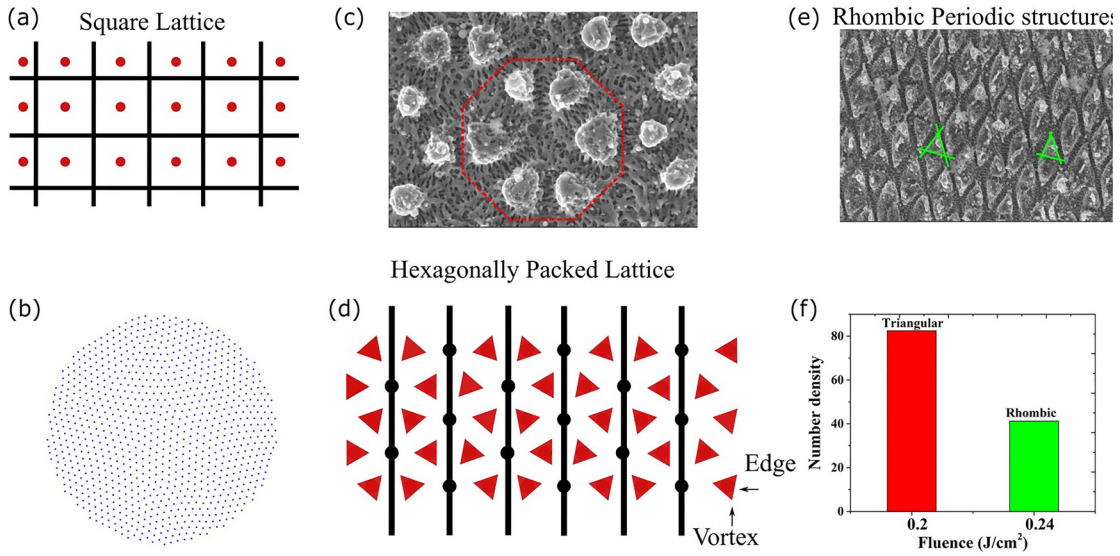

FIG. 3. Proposed mechanisms behind the formation of different 2D structures using two temporally delayed fs-laser pulses: (a) a schematic of particles forming in a square lattice due to the formation of orthogonal fs-LIPSSs following irradiation of orthogonal, temporally delayed pulses. (b) Theoretical calculation of particles originally situated in a square lattice and self-organizing in a hexagonal lattice due to columbic repulsion. (c) The experimentally obtained structures organized in a honeycomb lattice, i.e., a hexagonal lattice without a center particle. (d) A schematic of the formed HPT structure as a consequence of ablating the center particle in a hexagon lattice, due to strong ablation associated with the second pulse. (e) Experimental observation for the coalescence of the triangular structures into the rhombic structures. (f) The number density of hexagonal triangle and rhombic structures at different fluences counted from $5 \times 5\ \mu m^2$ in Figs. 2(d) and 2(e). The number of rhombic structures is approximately half of the triangular structures, indicating that they are formed due to merging of two oppositely facing triangles.

$$\vec{a}_{i,n+1} = k\sum_{j\neq i}\vec{R}_{ji,n}/R^3_{ji,n} - \gamma\vec{v}'_{i,n} + \vec{F}_{boundary}/m, \quad (1)$$

$$\vec{v}_{i,n+1} = \vec{v}_{i,n} + \vec{a}_{i,n+1} \times dt,$$

$$\vec{R}_{i,n+1} = \vec{R}_{i,n} + \vec{v}'_{i,n} \times dt,$$

$$\vec{v}'_{i,n} = \left(3\vec{v}_{i,n} - \vec{v}_{i,n-1}\right)/2,$$

where $\vec{a}$, $\vec{v}$, *and* $\vec{R}$ are the vectors to represent the acceleration, velocity, displacement of each particle at different times and $\vec{F}_{boundary}$ is a repulsive force around the simulation boundary, which is equal to $-k'\hat{R}'/|R-R'|$. R is the radius of the 2D circle space we simulated, R' is the position vector of a given particle, k' is a constant, and $\hat{R}'$ is a unit vector. $\vec{F}_{boundary}$ is the force that restricts the particles from being pushed outside the simulation domain and does not exist in a real experiment; however, it will not influence the distribution of the particles at the center of our 2D simulation space, k, γ, and m are the coefficients to balance the equation but are set to unity in the calculations. $k\sum_{j\neq i}\vec{R}_{ji,n}/R^3_{ji,n}$ and $-\gamma\vec{v}'_{i,n}$ represent the Coulomb force and viscous force, respectively. $\vec{v}_{i,n}$ is the time-dependent particle velocity obtained from the second order Euler method.

The simulation results are shown in Fig. 3(b) and enable us to explain the hexagonally packed triangular structures. However, the experimentally obtained structures are organized in a honeycomb lattice, i.e., a hexagonal lattice without a center particle [Fig. 3(c)]. We believe that this is due to the strong ablation associated with the fs-LIPSSs formed due to the second pulse which, as shown in Fig. 3(d), overlaps with the centered structure. This is corroborated by previous investigations which showed that stronger ablation is associated with the second pulse.[20,33] Accordingly, HPT structures are formed due to a combination of the scattered surface-wave interference mechanism followed by self-organization of surface structures due to Coulomb repulsion.

As we increase the fluence, rhombic structures [Fig. 2(e)] are formed, which is likely a consequence of melting and merging the HPT structures based on two observations. First, some rhombic structures are diagonally split by the shorter diagonal, i.e., consist of two separated triangles as shown in the marked regions in Fig. 3(e) and also see supplementary material Fig. S6. Furthermore, the number of rhombic structures is approximately half the number of triangular structures [Fig. 3(f)].

The HSFL structures are formed with low fluences, near the damage threshold of the materials.[38] Similarly, in our experiments, HSFL appeared at long delay times where the lattice has cooled down from the first pulse substantially. This is particularly true for Co as it has a high electron-phonon coupling factor ($g = 93 \times 10^{16}\ W/m^3\ K$) compared to many transition metals such as nickel ($36 \times 10^{16}\ W/m^3\ K$), chromium ($42 \times 10^{16}\ W/m^3\ K$), and copper ($10 \times 10^{16}\ W/m^3\ K$) or noble metals such as silver ($3.6 \times 10^{16}\ W/m^3\ K$) and gold ($2.1 \times 10^{16}\ W/m^3\ K$).[40,41] The origin of HSFL requires further studies and has been attributed to the fabrication of twin boundaries, self-organization and coherent superposition of scattered and refracted waves, laser-induced surface plasma waves, surface oxidation and second harmonic generation, and coherent nanobubble formation in the subsurface region.[15,42]

Using multiple, temporally delayed pulses can enable the formation of more complex, more uniform subwavelength structures with a larger area of coverage.[30] Our work shows that it is important to scan

the parameter space of all of the variables that can influence the morphology of the formed structures, e.g., time delay and fluence. In our work, we showed that the spherical structures packed in a square lattice initially formed due to laser irradiation-surface wave interference of orthogonally polarized pulses. This was followed by the HPT structures, which formed structures due to self-organization driven by Coulomb repulsion. The rhombic structures formed due to merging between two existing triangular structures. Our work paves the way toward controllable large-scale fabrication of complex periodic surface structures with different geometries and organizations.

See the supplementary material for the methods and details of surface structures.

This work was financially supported by the National Natural Science Foundation of China (NSFC) (Nos. 91750205 and 11674178) and Bill & Melinda Gates Foundation (No. OPP1119542).

REFERENCES

[1]A. Y. Vorobyev and C. Guo, Appl. Phys. Lett. **92**, 041914 (2008).
[2]A. Vorobyev and C. Guo, Opt. Express **18**, 6455 (2010).
[3]A. Y. Vorobyev and C. Guo, Laser Photonics Rev. **7**, 385 (2013).
[4]B. Terris and T. Thomson, J. Phys. D **38**, R199 (2005).
[5]V. Berube, G. Radtke, M. Dresselhaus, and G. Chen, Int. J. Energy Res. **31**, 637 (2007).
[6]U. Yogeswaran and S.-M. Chen, Sensors **8**, 290 (2008).
[7]D. K. Gramotnev and S. I. Bozhevolnyi, Nat. Photonics **4**, 83 (2010).
[8]A. A. Tseng, J. Micromech. Microeng. **14**, R15 (2004).
[9]F. Watt, A. Bettiol, J. Van Kan, E. Teo, and M. Breese, Int. J. Nanosci. **4**, 269 (2005).
[10]M. Altissimo, Biomicrofluidics **4**, 026503 (2010).
[11]A. Vorobyev and C. Guo, Phys. Rev. B **72**, 195422 (2005).
[12]R. Jagdheesh, B. Pathiraj, E. Karatay, G. Romer, and A. Huis in't Veld, Langmuir **27**, 8464 (2011).
[13]J. Cheng, C.—S. Liu, S. Shang, D. Liu, W. Perrie, G. Dearden, and K. Watkins, Opt. Laser Technol. **46**, 88 (2013).
[14]R. Buividas, M. Mikutis, and S. Juodkazis, Prog. Quantum Electron. **38**, 119 (2014).
[15]J. Bonse, S. Höhm, S. V. Kirner, A. Rosenfeld, and J. Krüger, IEEE J. Sel. Top. Quantum Electron. **23**, 9000615 (2017).
[16]T. Yong Hwang and C. Guo, J. Appl. Phys. **111**, 083518 (2012).
[17]J. Wang and C. Guo, Appl. Phys. Lett. **87**, 251914 (2005).
[18]A. Vorobyev, V. Makin, and C. Guo, J. Appl. Phys. **101**, 034903 (2007).
[19]E. Skoulas, A. Manousaki, C. Fotakis, and E. Stratakis, Sci. Rep. **7**, 45114 (2017).
[20]S. A. Jalil, J. Yang, M. ElKabbash, S. C. Singh, and C. Guo, Appl. Surf. Sci. **471**, 516 (2019).
[21]A. Y. Vorobyev and C. Guo, Adv. Mech. Eng. **2**, 452749 (2010).
[22]A. Vorobyev and C. Guo, J. Appl. Phys. **104**, 053516 (2008).
[23]A. Vorobyev and C. Guo, Opt. Express **19**, A1031 (2011).
[24]S. Höhm, A. Rosenfeld, J. Krüger, and J. Bonse, Opt. Express **23**, 25959 (2015).
[25]J.-M. Romano, A. Garcia-Giron, P. Penchev, and S. Dimov, Appl. Surf. Sci. **440**, 162 (2018).
[26]F. Fraggelakis, G. Mincuzzi, J. Lopez, I. Manek-Hönninger, and R. Kling, Appl. Surf. Sci. **470**, 677 (2019).
[27]J. Cong, J. Yang, B. Zhao, and X. Xu, Opt. Express **23**, 5357 (2015).
[28]H. Qiao, J. Yang, F. Wang, Y. Yang, and J. Sun, Opt. Express **23**, 26617 (2015).
[29]Q. Liu, N. Zhang, J. Yang, H. Qiao, and C. Guo, Opt. Express **26**, 11718 (2018).
[30]S. A. Jalil, J. Yang, M. ElKabbash, S. C. Singh, and C. Guo, Opt. Lett. **44**, 2278 (2019).
[31]F. Fraggelakis, G. Giannuzzi, C. Gaudiuso, I. Manek-Hönninger, G. Mincuzzi, A. Ancona, and R. Kling, Materials **12**, 1257 (2019).
[32]P. Bizi-Bandoki, S. Benayoun, S. Valette, B. Beaugiraud, and E. Audouard, Appl. Surf. Sci. **257**, 5213 (2011).
[33]S. Höhm, M. Herzlieb, A. Rosenfeld, J. Krüger, and J. Bonse, Appl. Surf. Sci. **374**, 331 (2016).
[34]A. Borowiec and H. Haugen, Appl. Phys. Lett. **82**, 4462 (2003).
[35]M. Huang, F. Zhao, Y. Cheng, N. Xu, and Z. Xu, ACS Nano **3**, 4062 (2009).
[36]O. Varlamova, F. Costache, J. Reif, and M. Bestehorn, Appl. Surf. Sci. **252**, 4702 (2006).
[37]Y. He, J. Zhang, S. Singh, E. Garcell, A. Y. Vorobyev, B. Lam, Z. Zhan, J. Yang, and C. Guo, Appl. Phys. Lett. **114**, 133107 (2019).
[38]R. Stoian, D. Ashkenasi, A. Rosenfeld, and E. Campbell, Phys. Rev. B **62**, 13167 (2000).
[39]J. C. Butcher, *Numerical Methods for Ordinary Differential Equations* (John Wiley & Sons. New York, 2003), p. 85.
[40]B. Keene, Int. Mater. Rev. **38**, 157 (1993).
[41]J. Hohlfeld, S.-S. Wellershoff, J. Güdde, U. Conrad, V. Jähnke, and E. Matthias, Chem. Phys. **251**, 237 (2000).
[42]X. Sedao, M. V. Shugaev, C. Wu, T. Douillard, C. Esnouf, C. Maurice, S. P. Reynaud, F. Pigeon, F. Garrelie, and L. V. Zhigilei, ACS Nano **10**, 6995 (2016).